

RESEARCH ARTICLE

Comprehensive Analysis of Rotor Geometric Parameters and Skewing Methods in Flux-Switching Generators

Tugberk Ozmen¹, Tayfun Isikelekoglu², Said Tunahan Durmaz², Batı Eren Ergun², Nevzat Onat³,
Mehmet Onur Gulbahce²

¹Department of Electric and Energy, Manisa Celal Bayar University, Manisa, Türkiye

²Department of Electrical Engineering, İstanbul Technical University, İstanbul, Türkiye

³Department of Electrical and Electronics Engineering, Manisa Celal Bayar University, Manisa, Türkiye

Cite this article as: T. Ozmen, T. Isikelekoglu, S. Tunahan Durmaz, B. Eren Ergun, and N. Onat, "Comprehensive analysis of rotor geometric parameters and skewing methods in flux-switching generators," *Turk J Electr Power Energy Syst.*, Published online April 21, 2025. doi 10.5152/tepes.2025.25003.

ABSTRACT

Flux-switching generators (FSGs) are widely used in wind turbine applications, particularly within microgrids, due to their unique structural and operational advantages. However, the salient pole structures of their stator and rotor teeth result in high torque ripple, elevated harmonic content, and increased magnetic flux density in the stator and rotor teeth. These issues necessitate optimization of the machine's design parameters. This study investigates the effects of rotor pole skew (delta) and coil-pole pitch ratio (embrace) on the performance of a 260 W FSG operating at 1200 rpm and 200 Hz. A multi-slice skewing method was applied to the rotor to analyze its impact on average torque, torque ripple, and efficiency. The results reveal that variations in pole skew and coil-pole pitch ratio significantly affect torque, flux linkage, and induced voltage while also reducing magnetic stresses. Despite these improvements, the prominence of the second harmonic limits the effectiveness of the skewing angle on generator output parameters. Additionally, the influence of the number of rotor slices on output performance and manufacturing complexity was examined.

Index Terms— Flux-switching generator, multi-slice skewing, torque ripple

I. INTRODUCTION

Unlike traditional power grids, decentralized microgrids have gained prominence in recent years. Microgrids are more flexible in structure and are suitable for meeting local energy needs [1]. With microgrids, energy supply security is enhanced. On the other hand, they reduce energy production costs and support the goal of reducing carbon emissions [2].

Flux-switching generators have garnered significant research interest due to their fundamental attributes, including a robust and simple structure along with the capacity for high power and torque density [3]. Since they do not have any excitation mechanism in their rotor, they do not require systems such as brushes or slip rings [4]. These machines are commonly used in low-power wind generation applications within microgrids [5-8]. Flux-switching machines (FSMs) feature excitation and armature windings located in the stator, with

excitation achieved via windings and/or permanent magnets (PMs). This stator-based excitation classifies FSMs as stator-active machines, with the absence of an excitation mechanism in the rotor making them particularly suitable for high-speed applications [9]. Due to the salient rotor and stator structure of these generators, the harmonic content in their output values is high [10]. The performance metrics of such generators can be improved through certain structural enhancements. The primary reasons for the preference of FSGs in microgrids are their ability to provide high power density, achieve high efficiency, have a simple and robust structure, and operate over a wide speed range.

Space harmonics, arising from machine geometry, significantly influence the performance of electrical machines. Rotor skewing is one method commonly employed to mitigate the effects of space harmonics, particularly in induction machines [11] and PM machines

Corresponding author: Tugberk Ozmen, tugberk.ozmen@cbu.edu.tr



Content of this journal is licensed under a Creative Commons Attribution (CC BY) 4.0 International License.

Received: January 15, 2025
Revision requested: February 16, 2025
Last revision received: February 21, 2025
Accepted: March 7, 2025
Publication Date: April 21, 2025

[12]. Due to their salient structure, FSMs experience high cogging torque and space harmonics [9]. Various methods, such as rotor geometry adjustments [13-15], current control techniques [16], and enhancements in winding configurations [17], have been implemented to reduce these effects. Additionally, studies on skewing methods for FSMs are present in the literature [4, 18].

The performance of FSGs is significantly influenced by the rotor tooth side angle (delta) and the pole-arc to pole-pitch ratio parameters, which affect both torque generation and the losses of these machines. The rotor tooth side angle directly impacts magnetic flux linkage, influencing torque output and cogging torque characteristics. Fig. 1 illustrates the pole pitch, pole arc, and delta on the machine geometry. Studies have demonstrated that optimizing the rotor tooth side angle can enhance torque density and minimize cogging torque. This is crucial for smooth operation and reducing acoustic noise in FSGs [19]. Similarly, the pole-arc to pole-pitch ratio parameter affects the flux distribution within the machine. By adjusting this ratio during operation, the machine's flux-weakening capability and torque-speed characteristics can be improved, providing better control over its performance at high speeds [20, 21]. The combined optimization of rotor tooth side angle and the pole-arc to pole-pitch ratio has been found to further enhance performance by balancing magnetic saturation and reducing iron losses, leading to increased efficiency and reliability [22].

Recent advancements in multi-objective optimization algorithms have proven critical in enabling the simultaneous adjustment of these parameters to achieve desired performance criteria, such as high torque density and low cogging torque, thereby playing an essential role in machine design and optimization [23-25].

In this study, the performance of a FSG is evaluated using the ANSYS Electronics Desktop. The effects of the pole-arc to pole-pitch ratio and tooth side angle, which are rotor parameters, on the performance of an FSG with a rated speed of 1200 min^{-1} , a frequency of 200 Hz, and an output power of 260 W, were investigated using the finite element method (FEM). Moreover, the effects of skewing applied to the rotor of the generator on electromagnetic torque, torque ripple, and generator efficiency were examined. The obtained results were evaluated by comparing flux distributions and output parameters.

Main Points

- The impact of rotor skewing and multi-slice configurations on torque ripple, average torque, and efficiency in FSGs was comprehensively analyzed.
- Key design parameters, including the rotor tooth side angle and the pole-arc to pole-pitch ratio, were optimized to enhance performance and reduce magnetic stress.
- Despite improvements, the dominance of the second harmonic limits the effectiveness of skewing, highlighting the need for advanced design strategies like double-stator configurations.

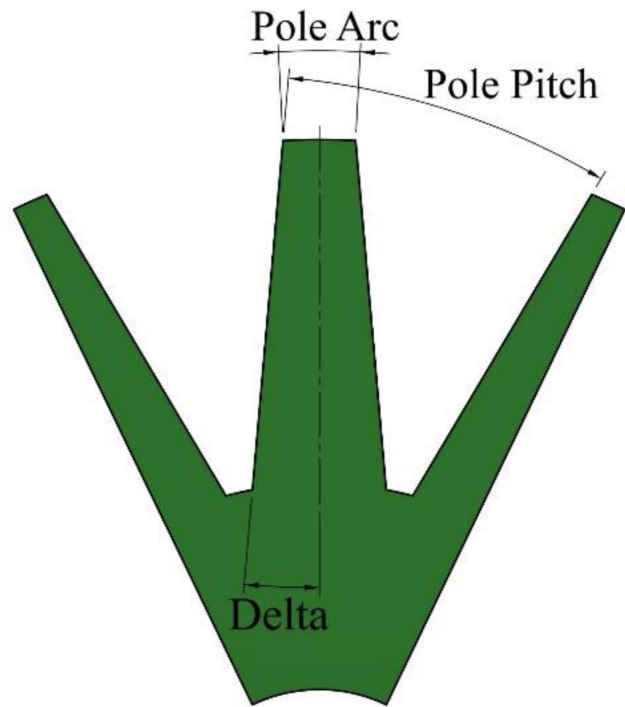


Fig. 1. Drawing of pole arc, pole pitch, and delta.

II. FLUX-SWITCHING GENERATORS

Flux-switching generators attract the interest of researchers due to their robust and simple structure, as well as their high power and torque density characteristics [3]. Flux-switching generators, which are used in low-power applications, are also preferred in wind turbines for microgrids [5, 26-28]. In FSGs, magnets and/or excitation windings are used for excitation. The excitation mechanisms are located in the stator, making it part of the active machine class. One of the key features of active stator machines is their suitability for high-speed applications, as they lack an excitation mechanism in the rotor [6]. Additionally, they offer high mechanical stability.

A) Operating Principle of Flux-Switching Generators

The operating principle of FSGs lies in the variation of the magnetic flux path and the associated magnetic reluctance as a function of rotor position. As the magnetic flux path changes, the flux linkage in the armature windings of the FSG varies, which induces a voltage.

Fig. 2 provides a visual illustration of the FSG's operation, depicting how the magnetic flux path changes relative to rotor position. As the magnetic flux path varies, both the magnitude and direction of flux linkage in the armature windings are altered. Consequently, a sinusoidal voltage is induced. To generate a complete sinusoidal voltage period, a single rotor tooth must traverse one stator slot pitch. Therefore, the number of poles in FSGs is determined by the number of rotor teeth.

B) Reference Flux-Switching Generator

The model of an FSG with a PM excitation, created in the 2D ANSYS-Maxwell simulation environment, is shown in Fig. 3. The rotor in the

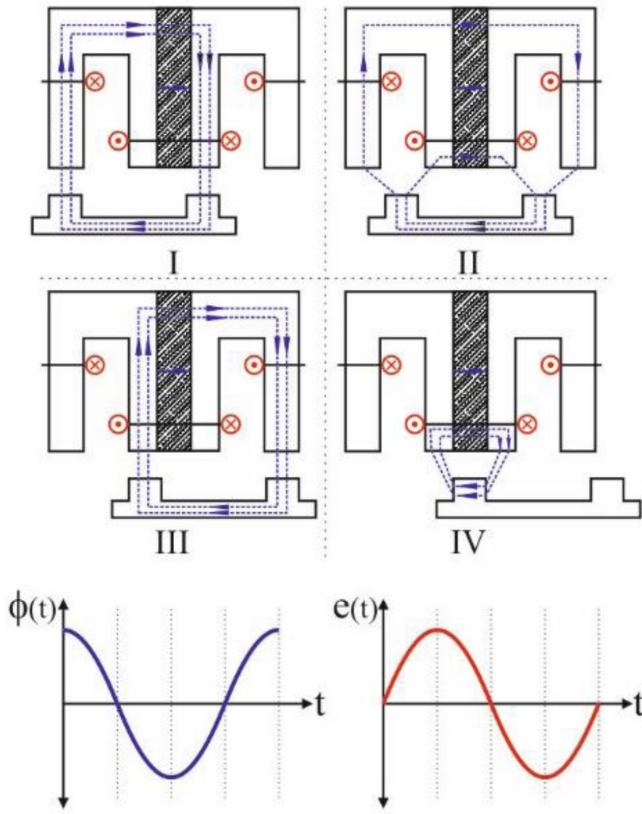


Fig. 2. Operating principle of flux-switching generators for a one-pole step diagram and magnetic flux-back emf waveforms.

simulated FSG model is composed of laminated sheets, while the stator features concentrated windings encircling axially magnetized PMs positioned between U-shaped segments.

To observe the effects of machine design parameters on output values more clearly, the generator provided in [29] is taken as a reference. The design parameters of the reference generator are provided in Table I. The slot-pole combination of the investigated FSG has a stator with 12 slots and a rotor with 10 poles (12/10p)—a commonly preferred structure in FSMs due to its reduced cogging

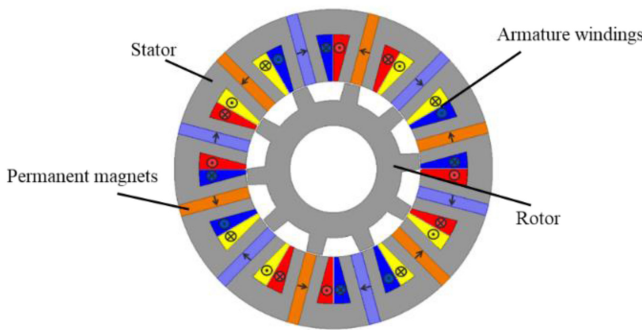


Fig. 3. The two-dimensional structure of the reference flux-switching generator.

TABLE I. DESIGN SPECIFICATIONS OF THE REFERENCE FLUX-SWITCHING GENERATOR

Parameter	Value
Stator slot number	12
Stator outer diameter (mm)	128
Rotor outer diameter (mm)	68.4
Length of air gap (mm)	1
Rotor pole number	10
Number of phase	3
Pole-arc to pole-pitch ratio	0.23
Magnet type	NdFe35
Rated speed (rpm)	1200

torque [30]. Two-dimensional transient magnetic analysis using the FEM has been applied to the generator, for which its design parameters are given in Table I. In this study, FEM analyses were carried out using the ANSYS Electronics Desktop. In the first stage of the design process, the geometric structure to be analyzed was modeled, taking into account the physical parameters.

Material properties suitable for each component were assigned to this model using the material library. After assigning the materials, the analysis boundaries and appropriate boundary conditions were defined, ensuring that the magnetic field distribution was accurately modeled. To enhance the solution accuracy of the model, a refined mesh structure was created in critical regions, such as

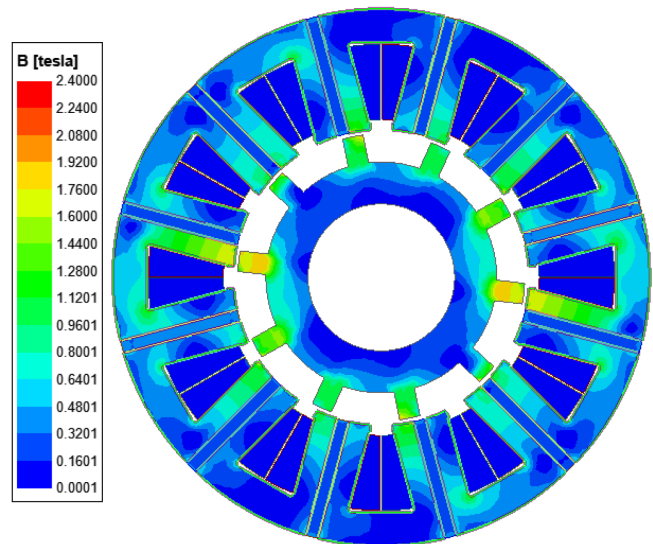


Fig. 4. Magnetic flux density distribution of the reference flux-switching generator.

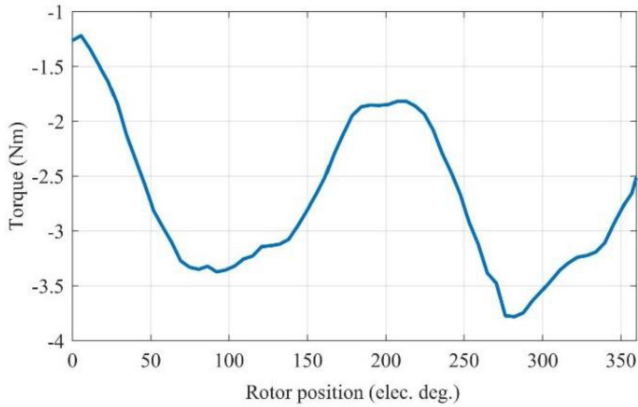


Fig. 5. Torque waveform of reference flux-switching generator.

the air gap, rotor tooth tips, and stator tooth tips, and appropriate mesh sizes were determined. For the time-dependent simulations of magnetic effects on the structure, the currents in the windings were defined as time-dependent functions. Finally, the required time steps for the analysis were determined, and the simulation setup was completed, after which the analysis was initiated. The magnetic flux density distribution of the reference generator is presented in Fig. 4. This graph shows that the highest magnetic

flux density is located at the stator and particularly at the rotor tooth tips.

To reduce magnetic saturation, improvements can be made in the machine geometry; in this context, the rotor tooth side angle and the pole-arc to pole-pitch ratio are key parameters that could optimize magnetic saturation.

The torque waveform of reference FSG is illustrated in Fig. 5. The average torque is measured at -2.64 Nm, with the torque ripple approximating the average torque at 2.58 Nm. Fig. 6(a) displays the radial component of the magnetic flux density and its harmonic spectrum in the air gap. Fig. 6(b) presents the harmonic content of flux density in the air gap. The rotor tooth aligns sequentially with

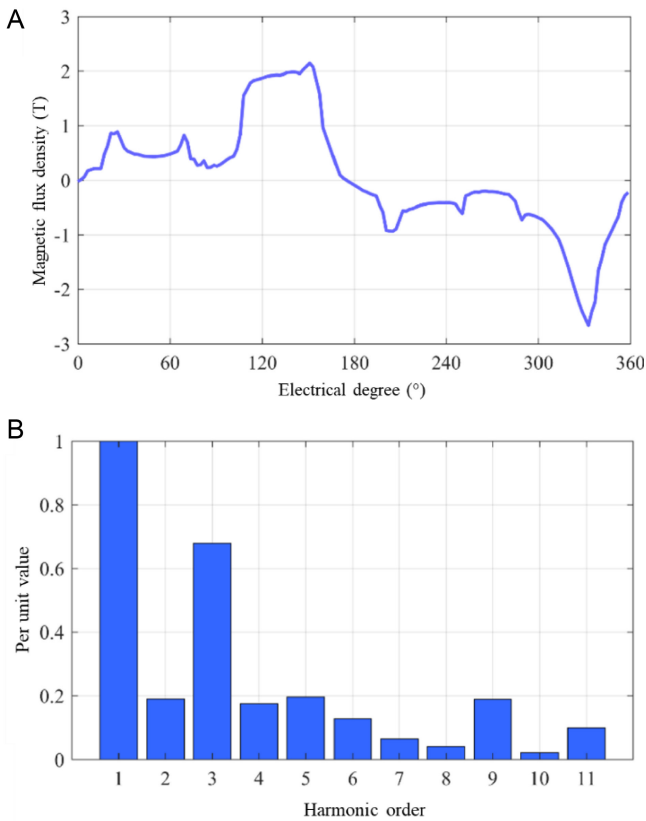


Fig. 6. Radial component of the magnetic flux density in the air gap (a) and its harmonic spectrum (b).

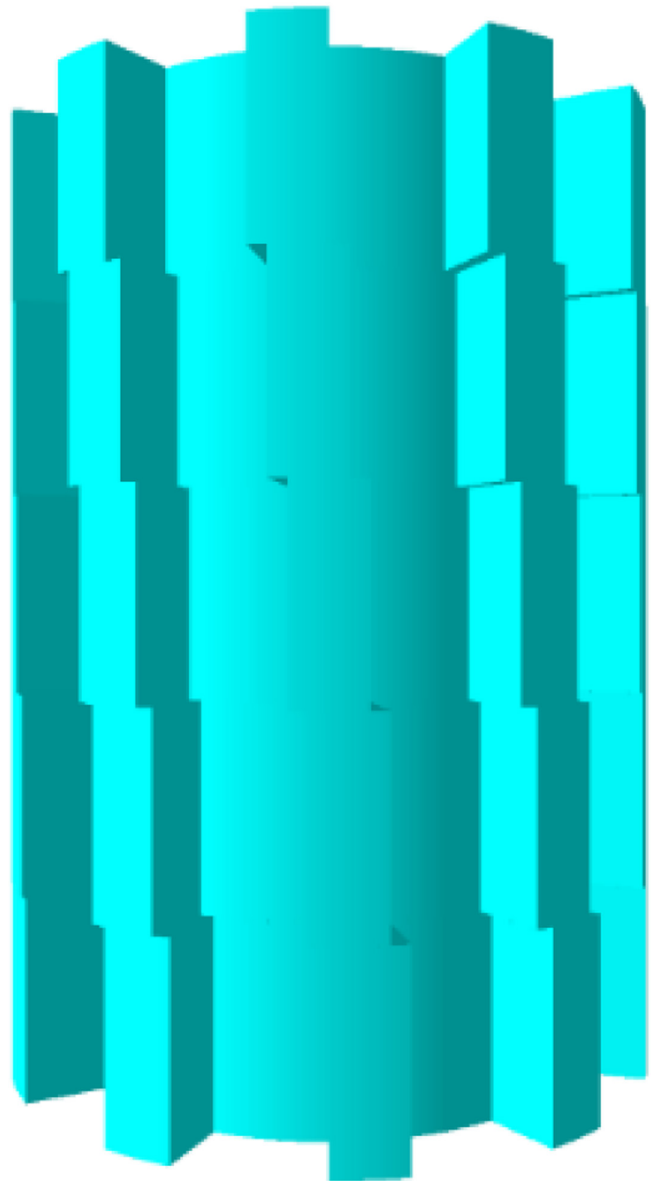


Fig. 7. Rotor with multi-slice skewing applied.

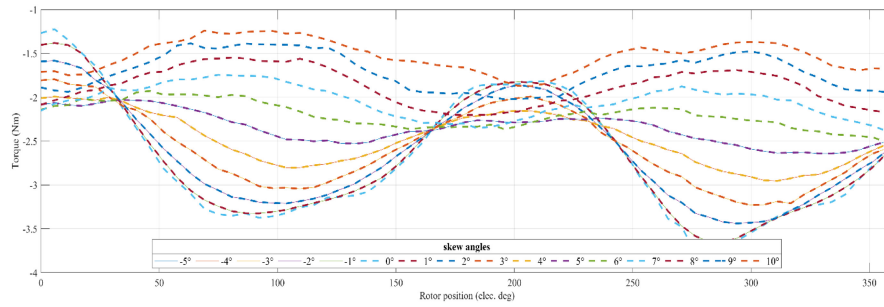


Fig. 8. Torque waveforms of flux-switching generator at different skew angles.

the stator tooth, slot opening, stator tooth, and PM during one electrical period. The permeability of the PM is similar to the slot gap’s permeability. Therefore, the permeance will experience two periods, while the flux linkage only has one period change. The effect of this situation is observed as the second harmonic. In machines where the second harmonic is dominant, the cogging torque remains significant even after applying rotor skewing.

III. THE IMPACT OF ROTOR GEOMETIC PARAMETERS ON PERFORMANCE OF FLUX-SWITCHING GENERATOR

A) The Impact of Multi-Slice Skewing

Flux-switching machines play a crucial role in modern electric machinery due to their high torque density, effective thermal

management—attributable to the placement of PMs in the stator—and robust rotor structure, which makes them well-suited for high-speed applications [31]. However, a notable drawback of FSMs is their inherent high torque ripple. The torque ripple in FSMs primarily originates from three key sources.

1. Cogging torque, which arises from variations in the magnetic field as the rotor position changes, causes the rotor to ‘lock’ at specific positions.
2. Torque is generated by the interaction between the magnetic fields of the winding currents and PMs.
3. Reluctance torque results from changes in winding inductance that vary with rotor position.

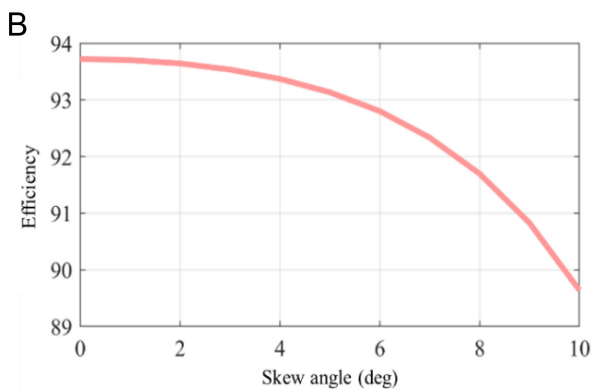
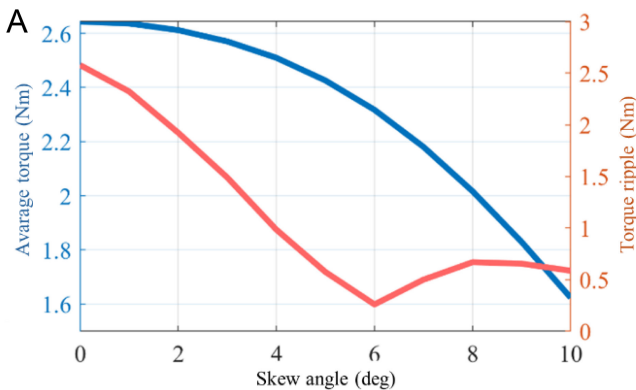


Fig. 9. The effects of each skewing angle on (a) average torque and torque ripple, (b) efficiency.

Additionally, the double-salient structure of FSMs contributes to magnetic saturation at the stator and rotor pole teeth, which induces periodic parasitic torque ripples that vary with rotor position [32]. Torque ripple can have detrimental effects, such as mechanical vibrations, acoustic noise, and energy losses. One of the most effective design techniques for mitigating harmonics in electromotive force and reducing torque ripple is skewing, which is applied in a multi-slice configuration to the reference FSM. In this multi-slice skewing method, the rotor is divided into equal-length sections along the rotor stack, with each section skewed at an identical angle, as illustrated in Fig. 7. Initially, the rotor was divided into five slices, and the impact of varying slice counts is explored in the subsequent sections.

Since the machine operates in generator mode, maintaining torque levels is crucial. Thus, skewing angles between 0° and 10° were analyzed. Additionally, for comparison, skewing angles as low as -5° were tested, with the results presented in Fig. 8. The analyzed values represent the skewing angle between the slices located at the two ends of the rotor. The analysis with a skewing angle of 0° serves as the baseline generator configuration.

Fig. 8 illustrates the effect of various skewing angles on torque. Some curves overlap, as applying skewing at equal but opposite angles yields the same effect. Fig. 9 shows the effects of each skewing angle on average torque, torque ripple, and efficiency. As the skewing angle increased, both average torque and efficiency decreased in a similar manner. Compared to the reference model without skewing, the average torque of the model with a 10° skew was reduced by approximately 38.57%.

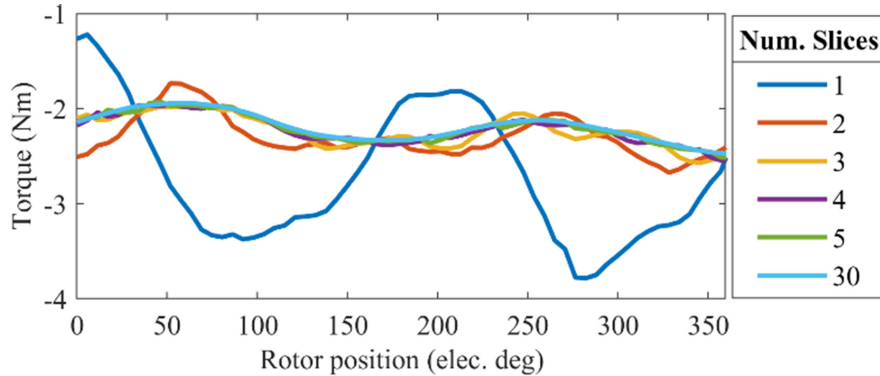


Fig. 10. Torque waveforms of FSG at different slice numbers.

The reduction in efficiency compared to the reference generator is 4.35%. As shown in the figures, torque ripple decreases up to a skewing angle of 6° , after which it begins to increase again. At a 6° skew, torque ripple was effectively reduced by 89.9% compared to the reference generator. In this case, the efficiency loss was 1.03%, and the reduction in average torque was 12.82%.

Studies have shown that increasing the number of skewing layers beyond a certain threshold yields limited improvements in performance [31]. To test this impact, the rotor structure was analyzed by fixing the skewing angle at 6° and varying the number of slices from 1 to 5. The case of a single-slice rotor represents the non-skewed condition, while a 30-slice rotor was also analyzed to observe the effects of excessive layering. The effect of increasing the number of rotor slices on torque variation is shown in Fig. 10. The corresponding values for average torque, torque ripple, and efficiency for different numbers of slices are presented in Table I.

As shown in Fig. 10, the layered structure applied to the rotor significantly impacts the torque ripple. According to Table II, the torque ripple for the single-slice structure is 2.58 Nm, which decreases to 0.38 Nm with the two-slice structure, representing an 85.4% reduction. However, when the number of slices exceeds two, the effect on torque ripple becomes limited.

TABLE II.
AVERAGE TORQUE, TORQUE RIPPLE, AND EFFICIENCY FOR
DIFFERENT NUMBERS OF SLICES

Number of Slice	Average Torque (Nm)	Torque Ripple (Nm)	Efficiency (%)
1	-2.64	2.58	93.72
2	-2.41	0.38	93.07
3	-2.30	0.39	92.90
4	-2.33	0.29	92.84
5	-2.32	0.26	92.80
30	-2.29	0.25	93.39

Table II shows that transitioning from a single-slice to a two-slice rotor structure led to a 0.7% decrease in efficiency. As the number of slices increased, efficiency generally declined; however, in the case of the 30-slice configuration, chosen to investigate multi-slice structures, efficiency slightly improved compared to structures with fewer slices. Applying a layered structure to the rotor also reduced the average torque. Alongside these results, the practicality of implementing a multi-slice structure should be assessed, particularly regarding its impact on electrical output parameters and manufacturability.

B) Effect of Rotor Tooth Side Angle and Pole-Arc to Pole-Pitch Ratio

The tooth side angle has an impact on the machine's electromagnetic performance, in particular. To observe this effect, tooth side angle values between 0° and 30° , with a step size of 5° , were selected and analyzed. The variation in torque, flux linkage and induced voltage based on the tooth side angle is presented in Fig. 11. An increase in the tooth side angle leads to a decrease in the average torque value.

As the tooth side angle increases, both the induced voltage and flux linkage also increase. The values of the generator output parameters based on the tooth side angle are presented in Table III. The magnetic flux distribution for the case where the tooth side angle is 30° is shown in Fig. 12.

Compared to the reference generator with a 0° tooth side angle, increasing this angle reduces the magnetic flux density in the rotor pole teeth.

The pole-arc to pole-pitch ratio is an important concept for the magnetic circuit of FSGs. This ratio indicates the extent to which the magnetic field covers the transmission paths within the machine. To ensure the smooth transmission of magnetic flux between the rotor and stator and to prevent magnetic leakage, the pole-arc to pole-pitch ratio must be optimized. By improving this ratio, the machine's efficiency increases, and energy losses are reduced. Therefore, optimizing the pole-arc to pole-pitch ratio during the design phase plays a critical role in the performance and longevity of the machine. Analyses were performed for the reference FSG with pole-arc to pole-pitch ratios of 0.15, 0.23, 0.30, and 0.40. The variation in torque, flux linkage, and induced voltage based on pole-arc to pole-pitch ratio is shown in Fig. 13.

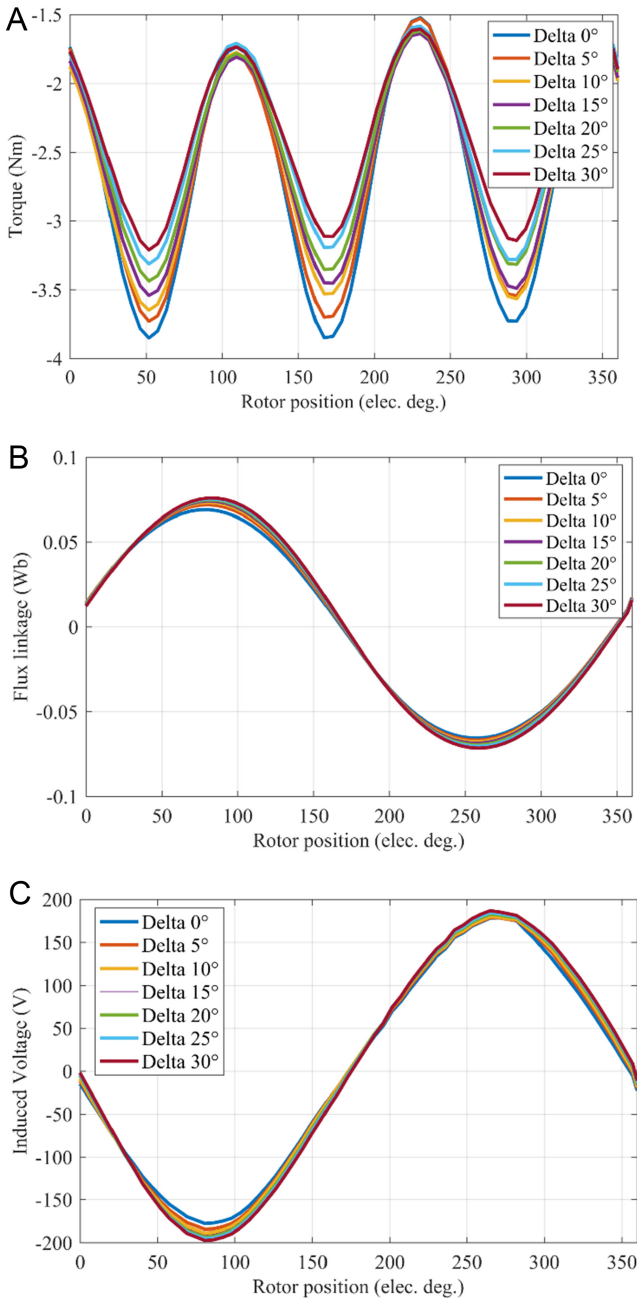


Fig. 11. The variation in (a) torque, (b) flux linkage, and (c) induced voltage based on the tooth side angle.

An increase in the pole-arc to pole-pitch ratio leads to a reduction in the average torque during generator operation. However, as the pole-arc to pole-pitch ratio increases, both the induced voltage and flux linkage also rise. Table IV presents the generator output parameters as a function of the pole-arc to pole-pitch ratio.

IV. CONCLUSION

Flux-switching generators are among the most promising candidates for variable-speed wind turbine applications due to their unique characteristics. Enhancements in output parameters such as power,

TABLE III.
OUTPUT VALUES BASED ON TOOTH SIDE ANGLE

Tooth Side Angle (°)	Induced Voltage (V)	Flux Linkage (Wb)	Torque (Nm)
0	121.02	0.048	-2.66
5	124.51	0.049	-2.61
10	126.50	0.050	-2.58
15	127.98	0.051	-2.56
20	129.22	0.051	-2.49
25	130.56	0.051	-2.40
30	132.11	0.052	-2.37

efficiency, and torque are critical to promoting their widespread use. In this study, a magnet-excited radial FSG with an output power of 260 W and a torque of 2.68 Nm was modeled and analyzed using the FEM.

To address torque ripple and optimize average torque, rotor skewing was applied. The results indicated that increasing the skewing angle led to a decrease in both average torque and efficiency, with the effect being more pronounced for torque. A 6° skew angle reduced torque ripple significantly by 89.9%, with a minimal efficiency reduction of just 0.98%. Additionally, it was observed that further increasing the number of rotor slices had limited influence on performance due to the dominance of the second-harmonic component. While the single-slice design produced the highest average torque, it also resulted in the highest torque ripple.

The study also investigated the effects of two key design parameters, namely the tooth side angle and the pole-arc to pole-pitch ratio, on generator performance. Increasing the tooth side angle from 0° to

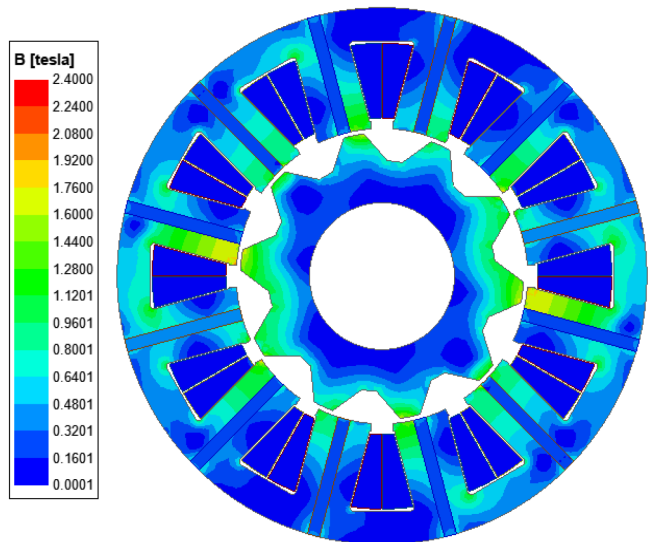


Fig. 12. Magnetic flux density distribution of the flux-switching generator when the tooth side angle is 30°.

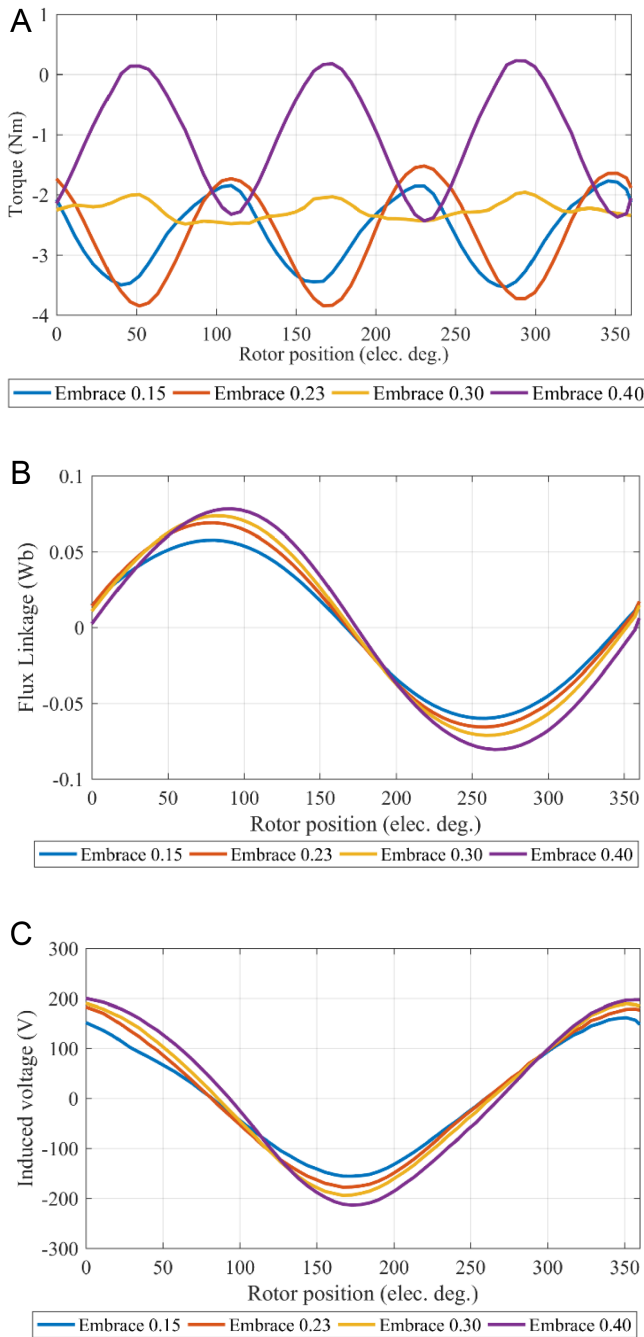


Fig. 13. The variation in (a) torque, (b) flux linkage, and (c) induced voltage based on pole-arc to pole-pitch ratio.

30° led to an approximate 11% reduction in torque but increased the induced voltage by 9.16%, resulting in an 8.33% increase in flux linkage. Similarly, increasing the pole-arc to pole-pitch ratio from 0.15 to 0.40 raised the induced voltage by 34.4% and flux linkage by 33.3%, but dramatically decreased torque by 62.4%. This highlights the trade-offs between these parameters and their impact on generator performance. Adjustments to these design parameters were also found to reduce magnetic stress in the FSG structure.

TABLE IV.
OUTPUT VALUES BASED ON THE POLE-ARC TO POLE-PITCH RATIO

Pole-Arc to Pole-Pitch Ratio	Induced Voltage (V)	Flux Linkage (Wb)	Torque (Nm)
0.15	105.70	0.042	-2.66
0.23	121.02	0.048	-2.66
0.30	130.43	0.051	-2.27
0.40	142.08	0.056	-1.00

The findings of this study indicate that the proposed FSG design, particularly with the optimized rotor skewing and pole-pitch ratio adjustments, holds significant potential for practical applications in low-power wind turbines and microgrid-based distributed generation systems. The reduction in torque ripple through multi-slice skewing is crucial for ensuring stable power generation and reducing mechanical vibrations in real-world implementations. Despite the improvements achieved through finite element simulations, a practical validation through experimental prototyping and real-world testing remains an important next step. Future research will focus on constructing a physical prototype to validate the simulation results, as well as assessing the manufacturability and efficiency of the proposed design under real operational conditions. Additionally, further studies will explore a double-stator model, which is expected to enhance machine performance by more effectively mitigating the second-harmonic component, thereby improving efficiency and reducing torque ripple even further.

Data Availability Statement

The data that support the findings of this study are available on request from the corresponding author.

Peer-review: Externally peer reviewed.

Author Contributions: Concept – T.O., T.I., S.T.D.; Design – S.T.D., T.I.; Supervision – B.E.E., M.O.G., N.O.; Resources – T.O., T.I., S.T.D.; Materials – T.I., S.T.D.; Data Collection and/or Processing – T.I., S.T.D.; Analysis and/or Interpretation – B.E.E., T.I., S.T.D., M.O.G.; Literature Search – T.O.; Writing Manuscript – T.O., T.I., S.T.D., M.O.G.; Critical Review – M.O.G., N.O.

Declaration of Interests: Mehmet Onur Gülbağçe is a member of the Advisory Board of Turkish Journal of Electrical Power and Energy Systems. However, his involvement in the peer review process was solely as an author. Other authors have no conflicts of interest to declare.

Funding: This work was supported in part by the 3501 Career Development Program of the Scientific and Technological Research Council of Turkey (TUBITAK) under Grant 124E306.

REFERENCES

1. P. Ramtekkar, and J. Chaudhari, "A novel design aspects of hybrid micro grid towards improved power quality issues," in IEEE 9th International Conference for Convergence in Technology (I2CT), Pune, India, April 5–7, 2024, 2024, pp. 1–4. [\[CrossRef\]](#).

2. T. G. Workineh, Y. B. Jember, and T. T. Yitayew, "Optimal design of hybrid micro-grid for productive use equipment: case of a rural town in ethiopia," in *IEEE PES/IAS PowerAfrica*, November 6–10, 2023, pp. 1–5.
3. J. Ojeda, M. G. Simões, G. J. Li, and M. Gabsi, "Design of a flux-switching electrical generator for wind turbine systems," *IEEE Trans. Ind. Appl.*, vol. 48, no. 6, pp. 1808–1816, 2012. [\[CrossRef\]](#)
4. T. Ozmen, B. E. Ergun, M. O. Gulbahce, and N. Onat, "Rare-earth magnet free flux-switching generator for wind turbines in micro-grids: A review," *Trans. Electr. Mach. Syst.*, vol. 8, no. 3, pp. 295–309, 2024. [\[CrossRef\]](#)
5. J. H. Yan, H. Y. Lin, Y. Huang, H. Liu, and Z. Q. Zhu, "Magnetic field analysis of a novel flux switching transverse flux permanent magnet wind generator with 3-D FEM," in *Proc. Int. Conf. Power Electron. Drive Syst.*, Taipei, Taiwan, November, 2-5, 2009, pp. 332–335. [\[CrossRef\]](#)
6. G. A. J. Amaratunga, P. P. Acarnley, and P. G. McLaren, "Optimum magnetic circuit configurations for permanent magnet aerospace generators," *IEEE Trans. Aerosp. Electron. Syst.*, vol. AES-21, no. 2, pp. 230–255, 1985. [\[CrossRef\]](#)
7. Y. Xu, C. Morito, and R. D. Lorenz, "Extending high-speed operating Range of induction machine drives using deadbeat direct torque and flux control with precise flux weakening," *IEEE Trans. Ind. Appl.*, vol. 55, no. 4, pp. 3770–3780, 2019. [\[CrossRef\]](#)
8. Z. Q. Zhu, and D. Howe, "Influence of design parameters on cogging torque in permanent magnet machines," *IEEE Trans. Energy Convers.*, vol. 15, no. 4, pp. 407–412, 2000. [\[CrossRef\]](#)
9. C. Sikder, I. Husain, and W. Ouyang, "Cogging torque reduction in flux-switching permanent magnet machines by rotor pole shaping," in *Proc. 2013 IEEE Energy Convers. Congr. Expo.*, Denver, CO, USA, IEEE, September 15–19, 2013, pp. 1555–1562. [\[CrossRef\]](#)
10. B. L. J. Gysen, E. Ilhan, K. J. Meessen, J. J. H. Paulides, and E. A. Lomonova, "Modeling of flux switching permanent magnet machines with Fourier analysis," *IEEE Trans. Magn.*, vol. 46, no. 6, pp. 1499–1502, 2010. [\[CrossRef\]](#)
11. D. H. Wang, X. H. Wang, and S. Y. Jung, "Reduction on cogging torque in flux-switching permanent magnet machine by teeth notching schemes," *IEEE Trans. Magn.*, vol. 48, no. 11, pp. 4228–4231, 2012. [\[CrossRef\]](#)
12. W. Xu, J. G. Zhu, Y. Zhang et al., "Cogging torque reduction for radially laminated flux-switching permanent magnet machine with 12/14 poles," in *Proc. IECON 2011-37th Annual Conf. IEEE Ind. Electron. Soc.*, Melbourne, Australia, November 7–11, 2011, pp. 3590–3595.
13. W. Xu, "Novel decoupling model-based predictive current control strategy for flux-switching permanent-magnet synchronous machines with low torque ripple and switching loss," *IEEE Trans. Appl. Supercond.*, vol. 24, no. 5, pp. 1–5, 2014.
14. H. Hwang, D. Kim, C. Lee, and H. Jin, "Torque ripple reduction in a flux-switching permanent magnet machine targeted at elevator door applications by minimizing space harmonics," in *Proc. 2016 IEEE Energy Convers. Congr. Expo. (ECCE)*, Milwaukee, WI, USA: IEEE, September 18–22, 2016, pp. 1–5. [\[CrossRef\]](#)
15. W. Fei, P. C. K. Luk, J. X. Shen, B. Xia, and Y. Wang, "Permanent-magnet flux-switching integrated starter generator with different rotor configurations for cogging torque and torque ripple mitigations," *IEEE Trans. Ind. Appl.*, vol. 47, no. 3, pp. 1247–1256, 2011. [\[CrossRef\]](#)
16. H. Ding, L. Zhang, A. Hembel, W. Lee, G. Nellis, and B. Sarlioglu, "Evaluation of the skewing effect on the electromagnetic and fluid mechanics performance of an integrated motor-compressor," *IEEE Trans. Ind. Appl.*, vol. 58, no. 1, pp. 273–283, 2022. [\[CrossRef\]](#)
17. F. Piriou, and A. Razek, "A model for coupled magnetic-electric circuits in electric machines with skewed slots," *IEEE Trans. Magn.*, vol. 26, no. 2, pp. 1096–1100, 1990. [\[CrossRef\]](#)
18. J. J. C. Gyselinck, L. Vandevelde, and J. A. A. Melkebeek, "Multi-slice FE modeling of electrical machines with skewed slots—The skew discretization error," *IEEE Trans. Magn.*, vol. 37, no. 5, pp. 3233–3237, 2001. [\[CrossRef\]](#)
19. S. Li, S. Zhang, T. G. Habetler, and R. G. Harley, "Modeling, design optimization, and applications of switched reluctance machines—A review," *IEEE Trans. Ind. Appl.*, vol. 55, no. 3, pp. 2660–2681, 2019. [\[CrossRef\]](#)
20. W. Hua, G. Zhang, and M. Cheng, "Flux-regulation theories and principles of hybrid-excited flux-switching machines," *IEEE Trans. Ind. Electron.*, vol. 62, no. 9, pp. 5359–5369, 2015. [\[CrossRef\]](#)
21. Y. Wang, and Z. Deng, "Comparison of hybrid excitation topologies for flux-switching machines," *IEEE Trans. Magn.*, vol. 48, no. 9, pp. 2518–2527, 2012. [\[CrossRef\]](#)
22. X. Sun, Y. Shen, S. Wang, G. Lei, Z. Yang, and S. Han, "Core losses analysis of a Novel 16/10 segmented rotor switched reluctance BSG motor for HEVs using nonlinear lumped parameter equivalent circuit model," *IEEE ASME Trans. Mechatron.*, vol. 23, no. 2, pp. 747–757, 2018. [\[CrossRef\]](#)
23. D. J. Evans, and Z. Q. Zhu, "Novel partitioned stator switched flux permanent magnet machines," *IEEE Trans. Magn.*, vol. 51, no. 1, pp. 1–14, 2015. [\[CrossRef\]](#)
24. E. Howard, M. J. Kamper, and S. Gerber, "Asymmetric flux barrier and skew design optimization of reluctance synchronous machines," *IEEE Trans. Ind. Appl.*, vol. 51, no. 5, pp. 3751–3760, 2015. [\[CrossRef\]](#)
25. H. Hua, and Z. Q. Zhu, "Novel partitioned stator hybrid excited switched flux machines," *IEEE Trans. Energy Convers.*, vol. 32, no. 2, pp. 495–504, 2017. [\[CrossRef\]](#)
26. O. Dobzhanskyi, P. Gottipati, E. Karaman, X. Luo, E. A. Mendrela, and A. M. Trzynadlowski, "Multilayer winding versus switched-flux permanent-magnet AC machines for gearless applications in clean-energy systems," *IEEE Trans. Ind. Appl.*, vol. 48, no. 6, pp. 2296–2302, 2012. [\[CrossRef\]](#)
27. M. Y. Lin, L. Hao, X. Li, X. Zhao, and Z. Q. Zhu, "A novel axial field flux-switching permanent magnet wind power generator," *IEEE Trans. Magn.*, vol. 47, no. 10, pp. 4457–4460, 2011. [\[CrossRef\]](#)
28. L. Hao, M. Y. Lin, X. M. Zhao, X. Fu, Z. Q. Zhu, and P. Jin, "Static characteristics analysis and experimental study of a novel axial field flux-switching permanent magnet generator," *IEEE Trans. Magn.*, vol. 48, no. 11, pp. 4212–4215, 2012. [\[CrossRef\]](#)
29. Y. Du et al., "Comparison of flux-switching PM motors with different winding configurations using magnetic gearing principle," *IEEE Trans. Magn.*, vol. 52, no. 5, pp. 1–8, 2016. [\[CrossRef\]](#)
30. J. Zhao, Y. Zheng, C. Zhu, X. Liu, and B. Li, "A novel modular-stator outer-rotor flux-switching permanent-magnet motor," *Energies*, vol. 10, no. 7, pp. 1–19, 2017. [\[CrossRef\]](#)
31. H. Chen, A. M. EL-Refai, and N. A. O. Demerdash, "Flux-switching permanent magnet machines: A review of opportunities and challenges—Part I: Fundamentals and topologies," *IEEE Trans. Energy Convers.*, vol. 35, no. 2, pp. 684–698, 2020. [\[CrossRef\]](#)
32. W. Fei, P. C. K. Luk, and J. Shen, "Torque analysis of permanent-magnet flux switching machines with rotor step skewing," *IEEE Trans. Magn.*, vol. 48, no. 10, pp. 2664–2673, 2012. [\[CrossRef\]](#)